Decentralized Control of Series Stacked Bidirectional DC-AC Modules

Prasanta K. Achanta, Dragan Maksimovic
Colorado Power Electronics Center
University of Colorado Boulder, CO 80309
Email: {prasanta.achanta,maksimov}@colorado.edu

Milan Ilic
Empower Micro Systems
Santa Clara, CA 95054
Email: Ilich@ieee.org

***Abstract*—This paper introduces a control strategy for series stacking of bidirectional single-phase dc-ac modules. The proposed control strategy achieves autonomous power sharing among the modules, without the need for a centralized controller. All the switching signals are local to the modules, all the modules are alike, and no high frequency control or communication lines are required between the modules. System advantages include autonomous bidirectional power sharing, scalability using low-voltage devices, and no need for high voltage dc wiring. The approach is verified by simulations of an 8-module 6 kW system, and by experiments on a prototype consisting of 100 W bidirectional single-phase dc-ac modules.**

I. Introduction

There is an increasing demand for integrating energy storage systems and distributed energy generation on the grid. In this regard, stacking low voltage inverter modules as shown in Fig. 1 has gained interest [1]–[6] due to system scalability without the need for high voltage dc wiring, as well as high efficiency due to reduced voltage gain per module and use of low-voltage devices. Series ac stacking using a central controller, as described in [1], requires high frequency switching signals to be sent from the central controller to each module. Dc-ac modules stacked as a series-ac parallel-dc system was suggested in [2], but experimental results and analysis were not provided. An autonomous control strategy, which models the output ports of the unidirectional modules as power sources is described in [3]. Another control strategy, which models one module as a current source and the rest as voltage sources is described in [4]. In this approach, not all the modules are the same, which adversely affects the modular plug-and-play features of the system.

The control strategy described in this paper overcomes all the aforementioned disadvantages. Decentralized control with no high frequency communication between the modules eliminates the need for a centralized or master controller. Furthermore, the system is uniquely capable of handling bidirectional power flow, which has not been addressed in prior works [1]–[8]. The same control scheme for processing power in both directions eliminates any discontinuities or complexities that may arise due to change in direction of power flow. The proposed control approach can be used for various applications including energy storage systems, PV systems with integrated energy storage, stand-alone off-grid systems, etc.

This paper is organized as follows. System operation and governing equations are described in Section II. The control architecture for autonomous power sharing, including bidirectional power flow, is discussed in Section III. Simulation results for a 8-module, 6 kW system along with a discussion of system stability is provided in Section IV. Experimental results for a prototype consisting of 100 W modules are provided in Section V. Section VI concludes the paper.

II. Series Stacked System Operation

As shown in Fig. 1, each module has two ports: A dc port and an ac port. Input to the dc port is a battery. The ac port

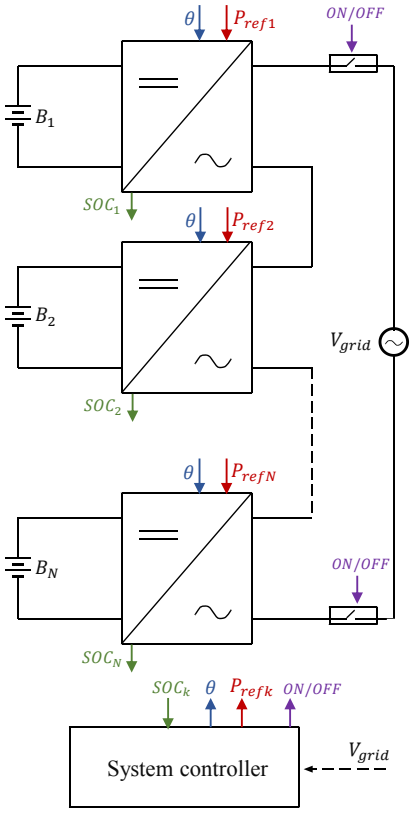

Figure 1: Series connected dc-ac modules. The modules can charge and discharge the batteries effectively operating as "ac batteries".

978-1-5386-1180-7/18/$31.00 ©2018 IEEE

is connected in series with the ac ports of other modules to add up to the desired grid voltage or to form an ac voltage in standalone operation. With the proposed control, the ac port behaves as a voltage source $V_{ref}\sin(2\pi 60t) \equiv V_{ref}\angle 0$, in series with a virtual droop resistor R_d.

To understand the working of each module, consider Fig. 2 and Fig. 3 with the ac port connected to an ac source $V_{in,ac}\angle 0$. When $V_{ref} > V_{in,ac}$, the battery discharges and the input port behaves as a power sink. When $V_{ref} < V_{in,ac}$ the battery is charged and the input port behaves as a power source. The current versus voltage characteristic of a single module is shown in Fig. 4. Several such modules can be connected in series to add up to the grid voltage as shown in Fig. 5. All modules share the same ac port current:

$$I_{ac} = \frac{(V_{ref1} + V_{ref2} + ... + V_{refN}) - V_{grid}}{NR_d} \quad (1)$$

and the output voltage of module n can be found as

$$V_{o,n} = V_{refn} - I_{ac}R_d \quad n \in 1, 2, 3...N \quad (2)$$

The output power P_n of module n is

$$P_n = \frac{V_{o,n}\angle 0 \;\; I_{ac}\angle 0}{2} \quad (3)$$

Given the fact that all the modules share the same ac current, the power processed by each module is in proportion to the voltage across the ac port of the module, and the corresponding dc port current is

$$I_{dcn} = \frac{P_n}{V_{dcn}} \quad (4)$$

The modules can be directed to produce (or absorb) different power levels, for example in order to enable balancing of the state of charge (SOC) of the battery modules connected to the dc ports, as shown in Fig. 1. With the power and voltage controls performed autonomously within each module, as described in the next section, a system controller only needs to perform high-level control functions, which do not require high-speed or time-critical communications with the modules. In particular, the system controller typically performs grid voltage sensing and synchronization, and delivers a line synchronization signal θ to the individual modules. In addition, the system controller may direct the modules to generate (or receive) different power levels in response to individual battery module SOC_k. Finally, as shown in Fig. 1, the system controller would typically assume the system connect/disconnect functions.

III. CONTROL ARCHITECTURE

The control strategy implemented inside each module is shown in Fig. 6, and a description of each block is given in Table I. A voltage reference signal V_{ref}, obtained from the corresponding power reference P_{ref}, is multiplied by a sinwave signal synchronized to the grid voltage. The reference for the module output voltage is finally obtained by subtracting a signal proportional to the output current, which implements the virtual droop resistance R_d. The output voltage is closed-loop regulated by a standard voltage control loop using a voltage-loop compensator G_c. It is assumed that the controller architectures and parameters are the same in all modules.

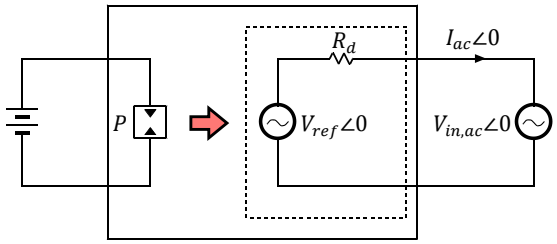

Figure 2: Model of a single module in discharge mode

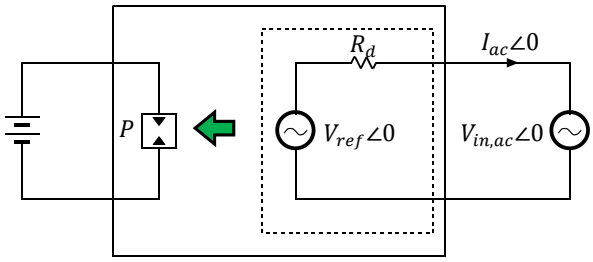

Figure 3: Model of a single module in charge mode

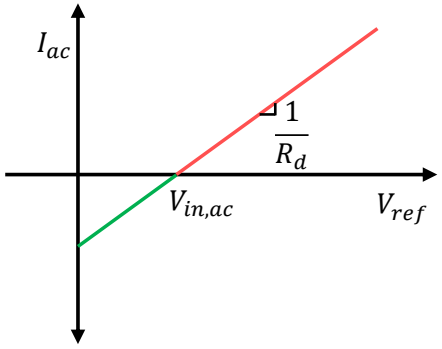

Figure 4: Characteristic plot of a single module

The design of the controller can be divided into three steps:

1) *Voltage control loop*: using the control-to-output voltage transfer function G_{vd} of the step-down power stage, compensator G_c is designed to achieve sufficient bandwidth and phase margin in the voltage control loop [9].
2) *Introducing virtual droop resistor*: the sensed output current is passed through a gain block containing droop resistance R_d to modify the reference command to the voltage control loop. This gain block along with the voltage controller ensure that the output port looks like a voltage source in series with the droop resistance.
3) *Generating the reference signal*: the amplitude of the reference command V_{ref} in each module determines the direction and magnitude of the power flow. A PLL, such

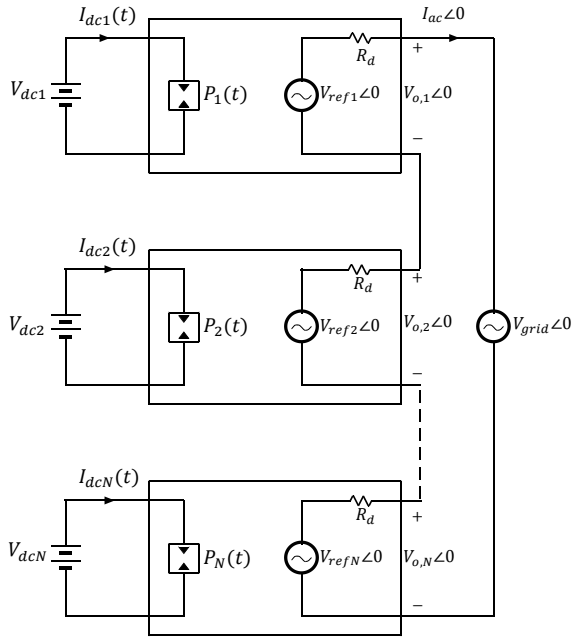

Figure 5: System model of series stacked dc-ac modules

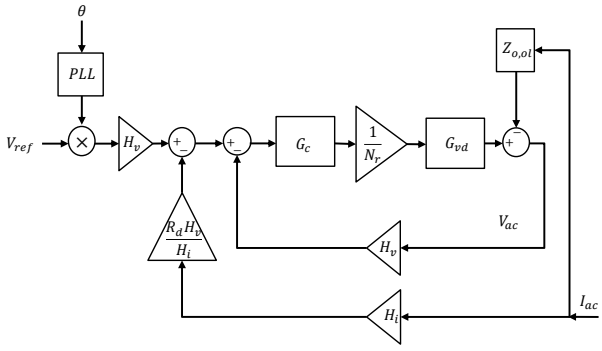

Figure 6: Block diagram of the droop control architecture

as the approach described in [10], is used to lock to the grid frequency using the synchronization signal θ.

The control architecture and the design approach are validated by simulations and experiments in the next two sections.

IV. Simulation Results

Consider a 6 kW system with 8 modules in series connected to a single phase 240 V_{rms} grid. The resulting system has a nominal output voltage of 30 V_{rms} per module. The system controller acts upon the system power command and outputs a power reference command P_{refk} to each of the modules. The system controller makes sure that the power demand is met while balancing the state of charge (SOC) of all the batteries, or performing other mismatch mitigation functions. The system controller is also responsible for providing the grid angle information θ to the modules. Note that this communication can be done at a much lower speeds compared to the bandwidth of the controllers present in the modules. A droop resistance of 0.214 Ω and a grid impedance of $Z_g = R_g + sL_g$ where $R_g = 60\,m\Omega$ and $L_g = 1$ mH was used in the system simulations. The control architecture shown in Fig. 6 is implemented in each module. The compensator G_c takes the form of a simple PI controller with K_p = 0.02 V^{-1} and K_i = 1257 $[\mathrm{Vs}]^{-1}$.

Table I: Description of the blocks used in the control architecture

$G_{v,d}$	Control-to-output voltage transfer function
G_c	Compensator transfer function
H_v	Voltage sensing gain
H_i	Current sensing gain
N_r	Gain of the pulse width modulator
R_d	Droop resistance
$Z_{o,ol}$	Open loop output impedance

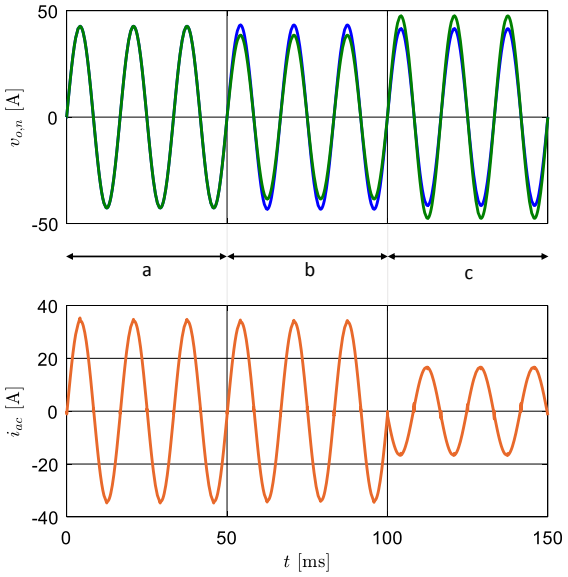

Figure 7: Top: Output voltage of the module with low SOC shown in green, output voltage of rest of the modules shown in blue. Bottom: Grid current

A. System operation

The simulation results shown in Fig. 7 demonstrate operation in three different modes of the system:

a. The system controller provides the same reference command of 750 W to all the modules. Voltage across all the modules is equal, suggesting equal power processing by all the modules.

b. In response to a low state of charge on one of the battery modules, the system controller lowers the reference

command on the corresponding module to 670 W. To meet the system power demand of 6 kW, the system controller also increases the reference command on the rest of the modules to 762 W. The output voltage across the module with the lower SOC drops indicating lower output power and correspondingly reduced battery discharge current. The grid current remains constant, confirming the ability of the system to meet the power demand despite module mismatches.

c. The system enters charging mode with P_{sys} = -3 kW evident from the 180 °shift of the ac current waveform. During the charging mode, the system controller makes sure that the module with the lower SOC receives a higher share of the incoming power, which is evident from the higher amplitude of the corresponding module's voltage waveform shown in green in Fig. 7.

Overtime, the system controller helps balance the state of charge of all the batteries, effectively working as a battery management system.

B. System stability

Stability of the series stacked system connected to the grid can be analyzed by looking at the impedance at the point of common coupling [11], [12]. With the proposed control scheme, the closed loop output impedance of each module $Z_{o,cl}$ is given by

$$Z_{o,cl} = \frac{T_i + Z_{o,ol}}{1 + T_v}, \tag{5}$$

where

$$T_i = \frac{G_c G_{vd} R_d H_v}{N_r} \tag{6}$$

and

$$T_v = \frac{G_c G_{vd} H_v}{N_r} \tag{7}$$

At low frequencies, $Z_{o,ol} \ll T_i$ and $T_v \gg 1$ making $Z_{o,cl} \approx R_d$. This shows the closed loop output impedance of each module at low frequencies looks like a resistance with a value equal to R_d. Each module sees the grid impedance ($Z_g = R_g + sL_g$) plus the closed loop output impedance of the other (N-1) modules. From Fig. 8 and Fig. 9, it is clear that there is sufficient phase at the point of common coupling, thus ensuring system stability.

V. EXPERIMENTAL RESULTS

Fig. 10 shows the experimental setup for a series stack of two modules. The parameters of each module are listed in Table II. The power stage of a single dc-ac module is shown in Fig. 11. The power stage consists of four switches $S_{HS1}, S_{LS1}, S_{HS2}, S_{LS2}$. During the positive half of the output ac cycle, S_{HS1}/S_{LS1} switch at fast PWM frequency while S_{LS2} remains turned ON. During the negative half of the output ac cycle, S_{HS2}/S_{LS2} switch at the fast PWM frequency while S_{LS1} remains turned ON. Each module is rated at 100 W and is implemented using EPC2102 GaN devices switching at 500 kHz, which results in small filter component values.

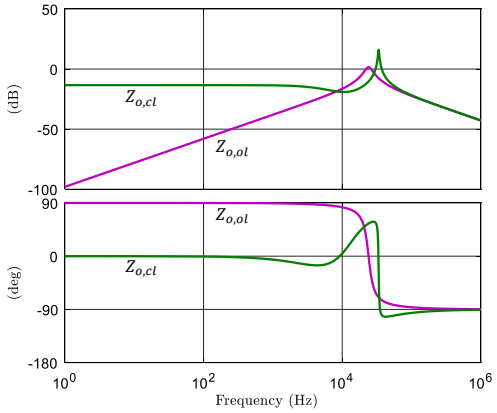

Figure 8: Bode plots of open loop and closed loop output impedance of a single module

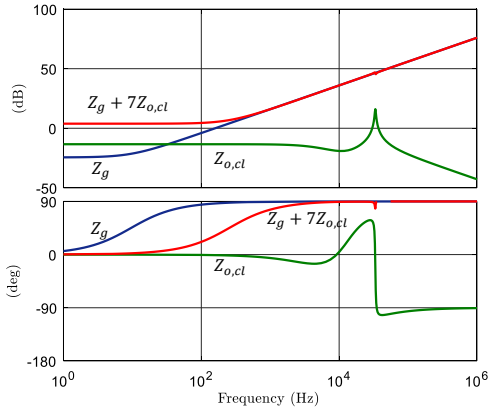

Figure 9: Bode plots of closed loop output impedance and the impedance seen by each module for N = 8

A simple digital PI compensator

$$G_c(z) = K_p + \frac{K_i}{1 - z^{-1}} \tag{8}$$

is implemented in the microcontroller of each module [9]. Experimental results for the system in discharge mode and a step down in the system power are shown in Fig. 12. Results for unequal power sharing between modules, while maintaining system power are shown in Fig. 13. Power shuffling between the two modules is demonstrated in Fig. 14. Waveforms in Fig. 15 show a transition from charging mode to discharging mode with equal power sharing between the modules. The reference voltage command on each module is changed from 4 V_{pk} to 7.5 V_{pk} to achieve this transition. Note that since there is equal power sharing between the modules, the voltage across each of them is the same.

Experimental results demonstrating unequal autonomous power sharing during charging and discharging are shown in Fig. 16. To achieve this, the reference command was changed from 5.7 V_{pk} to 5 V_{pk} on one module and from 1.7 V_{pk} to 9 V_{pk} on the other module.

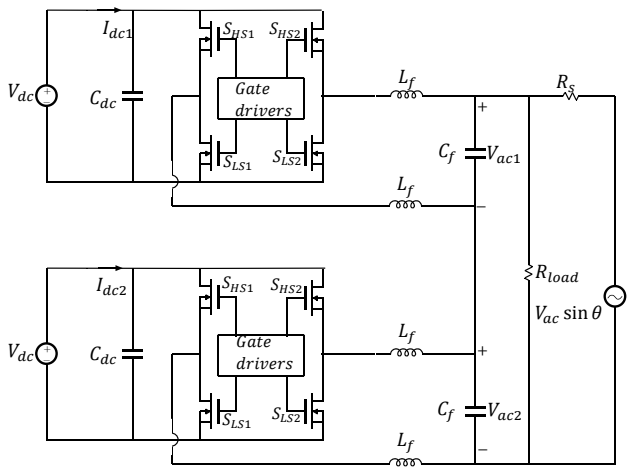

Figure 10: Experimental setup with two 100 W dc-ac modules connected in series

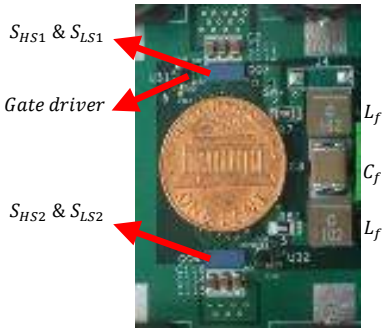

Figure 11: Power stage hardware of a 100 W bidirectional dc-ac module with GaN transistors and 9 V – 15 V dc input.

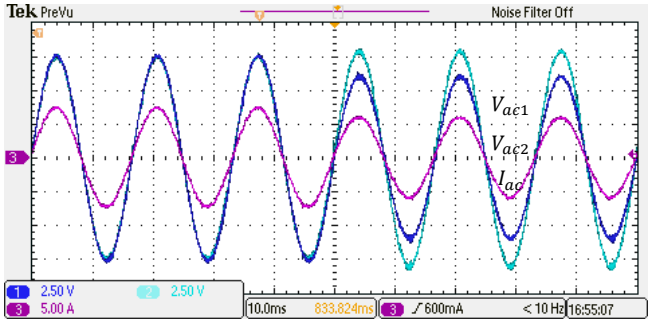

Figure 12: System transitions from P_{sys}: 50 W→38 W accompanied by unequal power processing between the modules. Note the drop in current amplitude showing a step down in system power. V_{ref1} : 10 V_{pk}, V_{ref2} : 10 V_{pk} → 8 V_{pk}

VI. CONCLUSIONS

This paper presents the design and implementation of a control scheme for series stacking of bidirectional low voltage dc-ac modules. The proposed system, which is capable of autonomous power sharing and bidirectional power flow, avoids high voltage dc wiring while providing benefits of modularity and scalability. The approach is verified by simulations on an 8-module 6 kW system tied to a 240 Vac grid, and by experiments on a scaled two-module system demonstrating power sharing and bidirectional power flow capabilities.

Table II: Values used in the experimental setup

Power FETs	EPC2102
Gate drivers	LM5113
Output capacitor C_f	22 μF
Output inductor L_f	1 μH
Microcontroller	TMS320F28069
Switching frequency	500 KHz
Droop resistance R_d	0.4 Ω
V_{dc}	10 V
R_{load}	2.8 Ω
R_s	1 Ω
V_{ac}	14.5 V
θ	2π60t

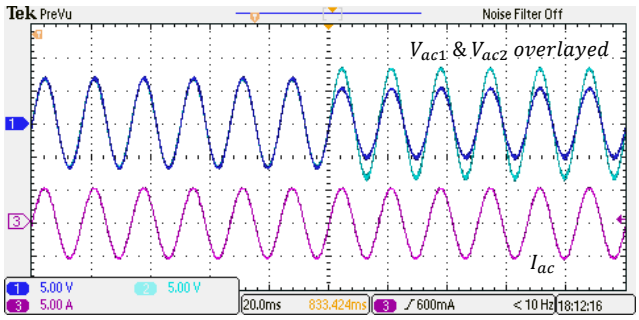

Figure 13: System transitions from equal power sharing between modules to unequal power sharing. Note that the system power remains constant throughout. V_{ref1} : 8.5 V_{pk} →10 V_{pk}, V_{ref2} : 8.5 V_{pk} → 7 V_{pk}

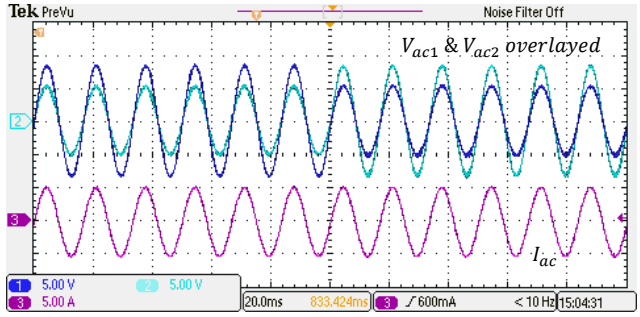

Figure 14: Unequal power sharing between modules while maintaining system power. V_{ref1} : 7 V_{pk} →10 V_{pk}, V_{ref2} : 10 V_{pk} → 7 V_{pk}

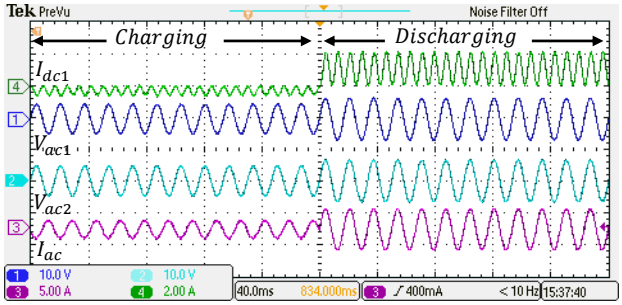

Figure 15: Equal power sharing during charging and discharging. Note that the output voltage of the modules V_{ac1} and V_{ac2} are out of phase with the output current I_{ac} during charging and in phase during discharging. $V_{ref1}: 4\,\mathrm{V}_{pk}, \rightarrow 7.5\,\mathrm{V}_{pk}$, $V_{ref2}: 4\,\mathrm{V}_{pk} \rightarrow 7.5\,\mathrm{V}_{pk}$

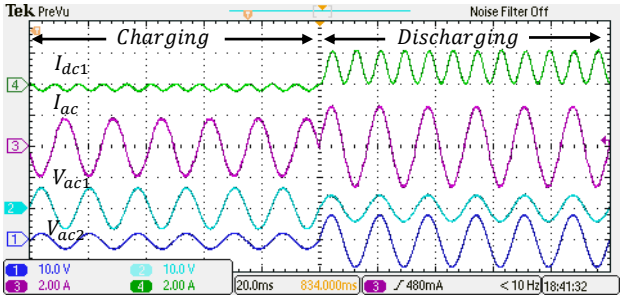

Figure 16: Unequal power sharing during charging and discharging. Note that V_{ac1} and V_{ac2} are different in amplitude because they are processing different power with the same output current I_{ac} passing through them.$V_{ref1}: 5.7\,\mathrm{V}_{pk} \rightarrow 5\,\mathrm{V}_{pk}$, $V_{ref2}: 1.7\,\mathrm{V}_{pk} \rightarrow 9\,\mathrm{V}_{pk}$

REFERENCES

[1] S. Kouro, B. Wu, . Moya, E. Villanueva, P. Correa, and J. Rodríguez, "Control of a cascaded h-bridge multilevel converter for grid connection of photovoltaic systems," in *Conf. IEEE Ind. Electron.*, pp. 3976–3982, Nov 2009.

[2] H. K. Krishnamurthy and R. Ayyanar, "Building block converter module for universal (ac-dc, dc-ac, dc-dc) fully modular power conversion architecture," in *Power Electron. Spec. Conf.*, pp. 483–489, June 2007.

[3] F. Lu, B. Choi, and D. Maksimovic, "Autonomous control of series-connected low voltage photovoltaic microinverters," in *Control Modeling Power Electron. (COMPEL)*, pp. 1–6, July 2015.

[4] H. Jafarian, I. Mazhari, B. Parkhideh, S. Trivedi, D. Somayajula, R. Cox, and S. Bhowmik, "Design and implementation of distributed control architecture of an ac-stacked pv inverter," in *Energy Conv. Cong. Exp. (ECCE)*, pp. 1130–1135, Sept 2015.

[5] B. Johnson, P. Krein, and P. Chapman, "Photovoltaic ac module composed of a very large number of interleaved inverters," in *Appl. Power Electron. Conf. Expo. (APEC)*, pp. 976–981, March 2011.

[6] M. Nuotio, M. Ilic, Y. Liu, J. Bonanno, and P. J. Verlinden, "Innovative ac photovoltaic module system using series connection and universal low-voltage micro inverters," in *Photovoltaic Spec. Conf. (PVSC)*, pp. 1367–1369, June 2014.

[7] C. Cecati, F. Ciancetta, and P. Siano, "A multilevel inverter for photovoltaic systems with fuzzy logic control," *IEEE Trans. Ind. Electron.*, vol. 57, pp. 4115–4125, Dec 2010.

[8] L. M. Tolbert and F. Z. Peng, "Multilevel converters as a utility interface for renewable energy systems," in *2000 Power Engineering Society Summer Meeting (Cat. No.00CH37134)*, vol. 2, pp. 1271–1274 vol. 2, 2000.

[9] L. Corradini, D. Maksimovic, P. Mattavelli, and R. Zane, *Digital Control of High-Frequency Switched-Mode Power Converters*. Piscataway, NJ: Wiley, 2015.

[10] M. Ciobotaru, R. Teodorescu, and F. Blaabjerg, "A new single-phase pll structure based on second order generalized integrator," in *Power Electron. Spec. Conf.*, pp. 1–6, June 2006.

[11] J. Sun, "Impedance-based stability criterion for grid-connected inverters," *IEEE Trans. Power Electron.*, vol. 26, pp. 3075–3078, Nov 2011.

[12] R. D. Middlebrook, "Input filter considerations in design and application of switching regulators," *IEEE Ind. Appl. Soc. Annu. Meeting*, pp. 366–382, 1976.